Electronic Supplementary Information

PAPER

Mapping nanoscale effects of charge traps on electrical transports in grain structures of indium tin oxide thin films

Received 9thJuly 2021,
Accepted 00th January 20xx

DOI: 10.1039/x0xx00000x

Hyesong Jeon[a], Jeongsu Kim[b], Shashank Shekhar[b], Jeehye Park[b] and Seunghun Hong[b*]

[a.] *Department of Materials Science and Engineering, Seoul National University, Seoul 08826, Korea.*
[b.] *Department of Physics and Astronomy, and Institute of Applied Physics, Seoul National University, Seoul 08826, Korea. E-mail: seunghun@snu.ac.kr*

†Electronic Supplementary Information (ESI) available: Calculation of sheet-resistance by a finite element method; Calculation of charge trap density by a resistance network model; Statistical distribution of charge trap density; Macroscopic current-voltage curves for untreated and plasma treated ITO; XRD, XPS and EDX spectra of untreated and plasma treated ITO; See DOI: 10.1039/x0xx00000x

1. Measurement geometry of an Indium Tin Oxide layer for scanning noise microscopy measurements

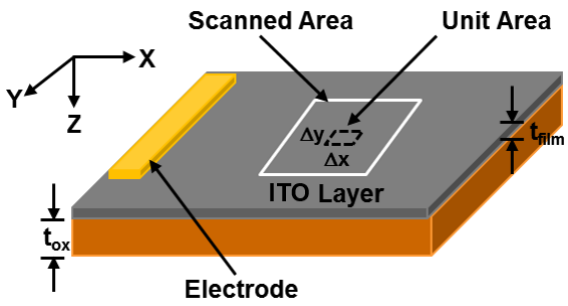

Fig. S1 The coordinate system of the ITO layer for scanning noise measurements. The ITO layer lies in the x-y plane. The t_{ox} denotes the thickness of the oxide layer. The t_{film} is the thickness of the ITO layer. The ΔxΔy is a unit area of the film denoting the size of the pixel (marked with dotted black lines). The total scanned area is marked with white lines. An area of or 3×3 μm² was scanned during measurements.

2. Calculation of Sheet Resistance Map on an ITO Layer

Fig. S1 shows a schematic diagram depicting an ITO layer measured *via* our noise–source imaging (NSI) system. A nanoscale conducting AFM probe made a direct contact on the ITO film and scanned the region marked by the solid white line ("scanned region"). While scanning, a constant bias voltage was maintained between the probe and the electrode, and the electrical current and the noise signals through the probe were measured to calculate the sheet resistance and noise–source distribution of the ITO film.

We developed an iterative method to calculate the sheet resistance distribution of the ITO film from the measured current map (Fig. 3b). Note that the current maps exhibited clear contrasts with a nanoscale resolution, implying that the variations of current values in the maps were determined by the localized sheet resistance values of the nearby ITO regions rather than those of far-away regions. Thus, in the case of Fig. S1, we can assume that the sheet resistance in the external region has a constant value, and the variation of sheet resistance values in the scanned region caused the variation of electrical currents through the probe. Then, the sheet resistance values of the external region and each point in the scanned region were calculated numerically using an iterative method as following.

As a first step, we calculated the sheet resistance value in the external region using an iterative method. Here, we assumed that the probe is placed at the centre of the scanned region and the entire ITO film has a uniform sheet resistance value of ~10 Ω/sq, which is a typical sheet resistance value reported in the literature. Then, the algorithms coded in Agros2D (http://agros2d.org) were used to calculate the electrical currents ($I_{simulation}$) through the probe. By using the Agros2D algorithms, the scalar electric potential $V(x, y)$ at each point of the ITO film was calculated by solving the quasi-harmonic equation as following (Eq. (S1)).[1]

$$\frac{\partial}{\partial x}\left(\frac{1}{R_s(x,y)}\frac{\partial V(x,y)}{\partial x}\right)+\frac{\partial}{\partial y}\left(\frac{1}{R_S(x,y)}\frac{\partial V(x,y}{\partial y}\right)=0 \quad \text{(S1)}$$

where $R_s(x, y)$ represents *the sheet resistance* at (x, y). Here, the boundary condition of a fixed potential $V(x, y)$ was applied to *the conducting probe* and *the electrode*, respectively. Also, a Neumann boundary condition of zero was imposed on the outer edges of the ITO film to prohibit currents flowing out of the ITO film. Then, the map of the electric field $E(x, y)$ on the ITO film was obtained by taking the gradient of the $V(x, y)$, and a current density $J(x, y)$ map could be obtained from the calculated E map using the relation

$$J(x,y)=\frac{1}{R_S(x,y)}E(x,y) \quad \text{(S2)}$$

Finally, the electrical currents $I_{simulation}$ through the probe could be calculated by integrating the current densities over the electrode surface. Then, we compared the $I_{simulation}$ with the averaged current value I_{avg} of the measured current map. If the $I_{simulation}$ was *higher* or *lower* than the I_{avg}, we recalculated $I_{simulation}$ assuming a *larger* or *smaller* R_{avg} value. We repeated the iteration using a secant algorithm[2] until we obtained a R_{avg} value to make the $I_{simulation}$ close to the I_{avg} with a less than 0.1% error.

The obtained R_{avg} was utilized as a sheet resistance value R_{ext} of the external region for the iterative calculation of the sheet resistance value at each point in the scanned region. Initially, we assumed a uniform sheet resistance $R_{scanned}(x, y) = R_{ext}$ in the scanned region, and the current $I_{simulation}(x, y)$ through the probe located at (x, y) was calculated using the same Agros2D algorithm. Then, $R_{scanned}(x, y)$ was adjusted following the secant algorithm until we obtained the sheet resistance value $R_{ini}(x, y)$ to make the $I_{simulation}(x, y)$ close to the current value $I_{measured}(x, y)$ in the measured current map with a less than 0.1% error. The calculation was repeated over all location (x, y) in the scanned region to obtain the map of sheet resistance value $R_{ini}(x, y)$ of the ITO film in the scanned region.

The obtained $R_{ini}(x, y)$ was used as an initial sheet resistance value at (x, y) for further simulation to calculate more precise sheet resistance value $R(x, y)$ of the ITO film in the scanned region. Here, we first assumed the uniform sheet resistance R_{ext} in the external region and the initial sheet resistance $R_{ini}(x, y)$ in the scanned region, and the electrical currents through the probe located at (x, y) were calculated using the Agros2D algorithm. Then, the sheet resistance value $R(x, y)$ of the ITO film at (x, y) was adjusted using a secant algorithm[2] until we obtained the sheet resistance value $R(x, y)$ to make the $I_{simulation}(x, y)$ close to the current value $I_{measured}(x, y)$ in the measured current map with a less than 10 % error. The calculation was repeated overall location (x, y) in the scanned region to obtain

the map of sheet resistance value R (x, y) of the ITO film at (x, y) in the scanned region.
Using the obtained sheet resistance map R (x, y), we performed the repeated calculation to update R (x, y) for more precise values. We repeated the calculation to continually update the sheet resistance value R (x, y) of the ITO film in the scanned region until the $I_{simulation}$ (x, y) over *all* points in the scanned region became close to the current value $I_{measured}$ (x, y) in the measured current map with a less than 10 % error. The obtained R (x, y) was used as a map of the sheet resistance of the ITO film in the scanned region.

3. Network Model for the Calculation of Noise-source Density Map on an ITO Layer

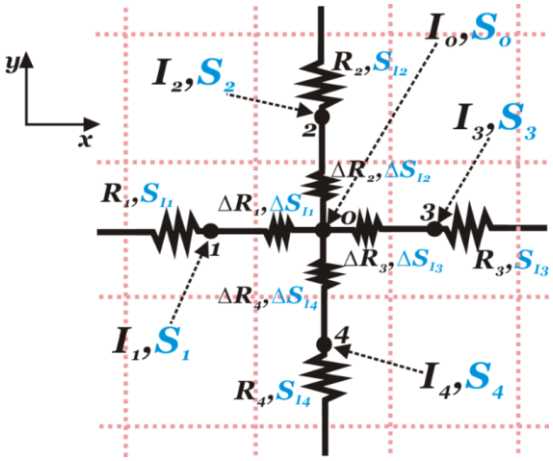

Fig. S2 Circuit diagram of the resistance network representing an ITO layer. The ITO channel was assumed as a resistor network. In our network model, every single node (node 0) is connected to its neighbour nodes (node 1, 2, 3, and 4) by a small resistance ΔR.

At first, let us consider a node 0 at (x, y) position as shown in Fig. S2. The node 0 is connected to four different nodes i (i = 1, 2, 3, and 4) through four small resistances ΔR_i. Each resistance generates the current noise ΔS_i. For square lattice, ΔR_i is the same as sheet resistance R_s of the ITO layer. Further, when ΔI is small, the variation of ΔR_i for a specific node is much smaller than ΔR_i. Thus, we can approximate all of ΔR_i (i =1, 2, 3, and 4) as their averaged value of ~ΔR, and the sheet resistance map obtained using our computational method could be utilized to obtain a ΔR_i value at node 0. The R_i (i =1, 2, 3, and 4) represents the effective resistance of the total current paths between node i and the metal electrode, excluding the current paths passing through node 0. Note that the finite element method simulation used to estimate the sheet resistance map provided the current density map, enabling the estimation of the I_1, I_2, I_3, and I_4. Using the values, the R_i values could be obtained using Ohm's law,

$$V = (R_i + \Delta R)I_i \tag{S3}$$

In our network model, all of the resistance components were assumed as independent noise sources, as shown in Fig. S2. In general, when two independent noise sources i (i = 1, 2) are connected in parallel, the total current PSD is given by

$$S_{total} = S_{I1} + S_{I2} \tag{S4}$$

On the other hand, when two independent noise sources are connected in series, the total current PSD is given by

$$S_{total} = \frac{S_{V1}+S_{V2}}{(R_1+R_2)^2} = \left(\frac{R_1}{R_1+R_2}\right)^2 S_{I1} + \left(\frac{R_2}{R_1+R_2}\right)^2 S_{I2} \tag{S5}$$

where R_i and S_{Ii} (i = 1, 2, 3, 4) correspond to the *resistance* and *generated current noise* of each resistance component with noise sources, respectively.
The Eqns. S4 and S5 imply that if we have local resistance information, we can calculate the current PSD for individual noise sources in the network system. Therefore, we could obtain the current PSD ΔS_I from the resistance ΔR, using the sheet resistance map. Here, S_{Ii} and ΔS_{Ii} correspond to the current PSD generated by the resistance components of R_i and ΔR_i, respectively. We can also approximate all of the ΔS_{Ii} as their averaged value ΔS.
The generalized calculation method of noise-source density is described in our previous report.[3] Here we briefly summarize the ITO-specific details and key equations.
The total power spectral density (PSD) of the mean-square fluctuation in the number of occupied charge traps per unit area $\Delta x\Delta y$ is given by[3-5]

$$\Delta S_{N_t}(f,x,y) \approx \Delta x\Delta y \cdot kT \cdot \int \frac{4\tau(E_f,x,y,z)}{1+[2\pi f\cdot\tau(E_f,x,y,z)]^2} \cdot N_t(E_f,x,y,z)\cdot dz \tag{S6}$$

Here, the $N_t(E, x, y, z)$ τ and τ are the density of the charge traps over the space and energy, a trapping time constant, and an angular frequency, respectively. The trap occupancy function is defined as $f_t = [1 + \exp(E - E_f) / kT]^{-1}$ where E_f is Fermi level. The coordination system and the structure of the ITO device were shown in Fig. S1.
In previous works, the integral over z ranged only to oxide thickness t_{ox}, and charge traps were considered to be buried in underlying oxide layers only. However, disordered sample such as ITO film can itself be the significant source of the traps. Thus, we defined an effective charge trap density N_{eff} as

$$N_{eff}(f,x,y) \equiv f \cdot \int \frac{4\tau(E_f,x,y,z)}{1+[2\pi f\cdot\tau(E_f,x,y,z)]^2} \cdot N_t(E_f,x,y,z)\cdot dz \tag{S7}$$

Then, the equation (S6) can be rewritten as

$$\Delta S_{N_t}(f,x,y) = \frac{kT}{f} N_{eff}(f,x,y)\cdot\Delta x\Delta y \tag{S8}$$

It follows that the current PSD per unit area $\Delta x\Delta y$ is

$$\Delta S_I(f,x,y) = \frac{(I)^2}{(\Delta C)^2}\Delta S_{N_t}(f,x,y) = \frac{(I)^2}{(\Delta C)^2}\frac{kT}{f} N_{eff}(f,x,y)\cdot\Delta x\Delta y \tag{S9}$$

where the ΔC is the number of charge carriers in the area of $\Delta x\Delta y$. Using the equation (S9), we can obtain the effective noise source density N_{eff} as,

$$\Delta S_{N_t}(f,x,y) = \frac{kT}{f} N_{eff}(f,x,y) \cdot \Delta x \Delta y \quad \text{(S10)}$$

The Eqn. S10 indicates that we can extract the information of the effective charge trap density directly from the current PSD per unit area. The capacitance of our ITO sample was estimated as ~1.38x10^{-7} C/V, and the threshold voltage was ~10 V. Thus, the total number of charge carriers in the ITO thin film was calculated as ~1x10^{12}. The total length and width of the ITO channel was ~2 cm, and the pixel size Δx and Δy of our measurement system was ~3.9 nm. Thus, the number of charge carriers in the area of $\Delta x \Delta y$ can be estimated as.

$$\Delta C \sim 1 \times 10^{12} \times \left(\frac{(3.9\times10^{-9})^2}{(0.02)^2}\right) \sim 0.26. \quad \text{(S11)}$$

Consequently, we have obtained the effective noise source density N_{eff} from the sheet resistance data and the local current PSD data, which could be directly measured by our noise–source imaging technique.

4. Statistical distribution of charge trap density

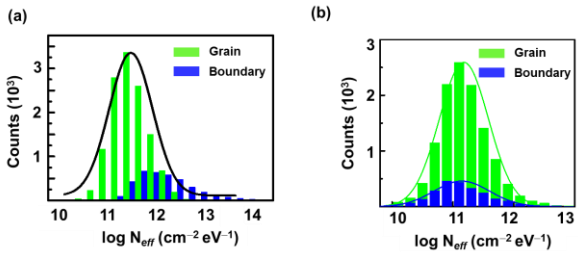

Fig. S3 Statistical distribution of charge trap density (N_{eff}) values of untreated and oxygen plasma-treated ITO thin film. (a) Histogram plots of N_{eff} of grains and boundaries of the untreated ITO. (b) Histogram plot of N_{eff} values for the grains and boundaries of the plasma treated ITO.

5. Topography image after plasma cleaning

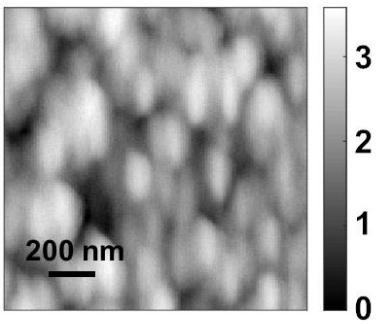

Fig. S4 Topography image of the plasma-treated ITO film shown in Fig. 4. The height variation and domains size did not change noticeably after the plasma treatment.

6. Current dependence on applied bias on a macroscopic measurement condition

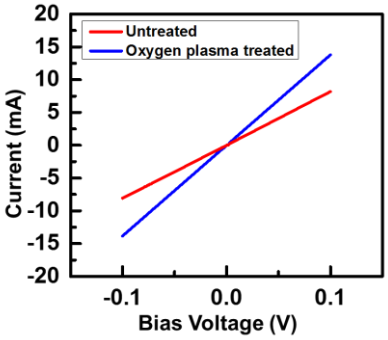

Fig. S5 Macroscopic I–V curve of the same ITO film before and after the oxygen plasma treatment. The current is increased by nearly two times after the oxygen treatment, which supports the results of the sheet conductance changes after the treatment.

7. X-ray diffraction spectra of untreated and plasma treated ITO films

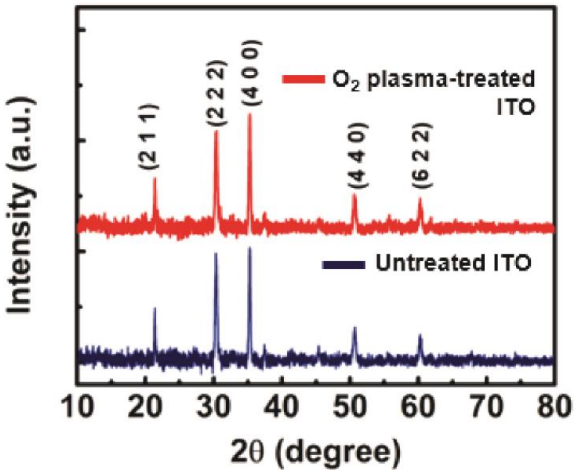

Fig. S6 XRD spectra of untreated ITO and oxygen plasma-treated ITO thin films. The intensity of peaks representing major planes of (211) and (222) increased after an oxygen plasma treatment. It indicates that the amounts of crystalline In_2O_3 and SnO_2 phases are increased.

8. X-ray photon-electron spectra of untreated and plasma treated ITO films

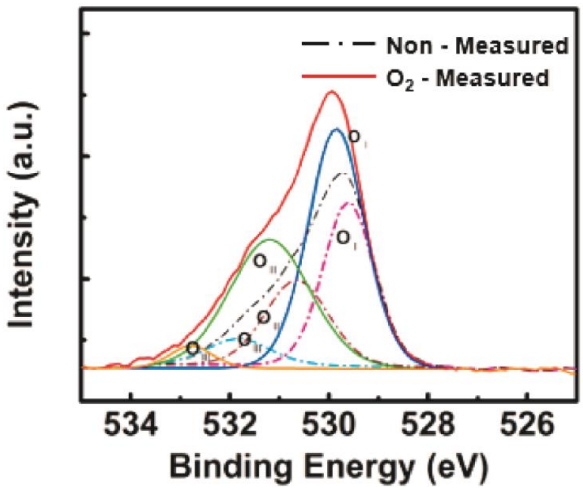

Fig. S7 XPS spectra of untreated ITO and oxygen plasma-treated ITO thin films. O_I and O_{II} peaks were attributed to an oxygen in an ITO lattice without and with oxygen vacancies, respectively. O_{III} peak represented chemisorbed oxygen atoms onto a surface, namely oxygen contaminants.

9. Energy dispersive X-ray spectra of grains and boundaries of untreated and plasma-treated ITO films

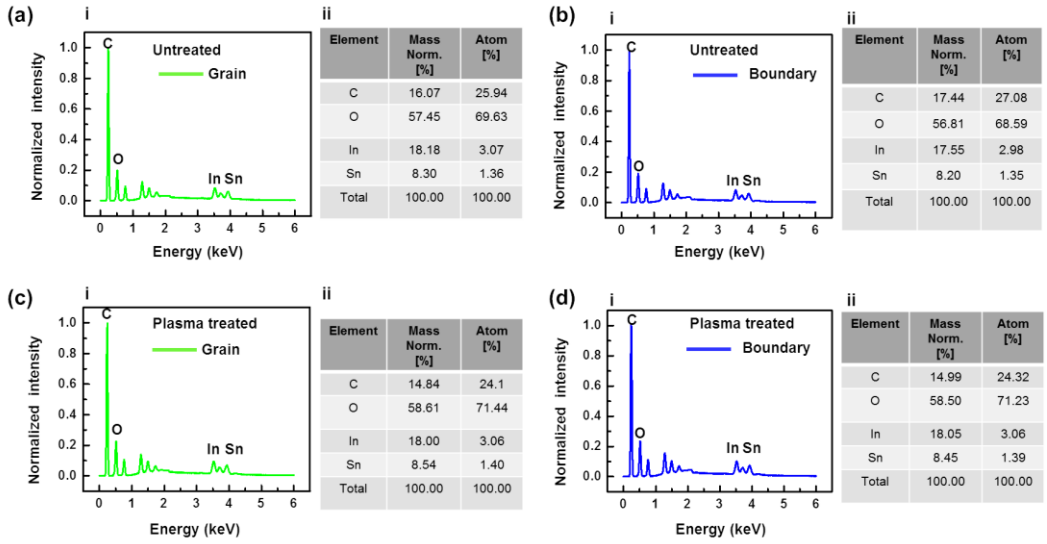

Element	Mass Norm. [%]	Atom [%]
C	16.07	25.94
O	57.45	69.63
In	18.18	3.07
Sn	8.30	1.36
Total	100.00	100.00

Element	Mass Norm. [%]	Atom [%]
C	17.44	27.08
O	56.81	68.59
In	17.55	2.98
Sn	8.20	1.35
Total	100.00	100.00

Element	Mass Norm. [%]	Atom [%]
C	14.84	24.1
O	58.61	71.44
In	18.00	3.06
Sn	8.54	1.40
Total	100.00	100.00

Element	Mass Norm. [%]	Atom [%]
C	14.99	24.32
O	58.50	71.23
In	18.05	3.06
Sn	8.45	1.39
Total	100.00	100.00

Fig. S8 EDS spectra of grains and boundaries of untreated ITO and oxygen plasma-treated ITO thin films. (a,b) EDS spectra of grain and boundaries of untreated ITO. The atomic percentage of oxygen was 69.63 and 68.59%, respectively. (c,d) EDS spectra of grain and boundaries of plasma treated ITO. The atomic percentage of oxygen increased to 71.44 and 71.23% in grains and boundaries, respectively. Also, there was decrease in the carbon percentages after the plasma treatment.

References

1 1. T. Mitsuhashi, K. Yoshida K, A Resistance calculation algorithm and its application to circuit extraction. *IEEE Trans. Comput*.-*Aided Des*. *Integr. Circuits Syst*. 1987, **6**, 337-45.

2 2. J. G. P. Barnes, An algorithm for solving non-linear equations based on the secant method. *The Comput*. *J*. 1965, **8**, 66-72.

3 3. H. Lee, D. Cho, S. Shekhar, J. Kim, J. Park, B. H. Hong, et al., Nanoscale direct mapping of noise source activities in graphene. *ACS Nano*, 2016, **10**,10135-10142.

4 4. K. K. Hung, P. K. Ko, C. M. Hu, Y. C. Cheng. A unified model for the flicker noise in metal oxide-semiconductor field-effect transistors. *IEE Tran*. *Electron Devices*, 1990, **37**, 654-65.

5 5. G. Reimbold, Modified *1/f* trapping noise theory and experiments in Mos-transistors biased from weak to strong inversion influence of interface states. *IEEE Tran*. *Electron Devices*, 1984, **31**,1190-1198.